Environmental Research 188 (2020) 109786

Contents lists available at ScienceDirect

Environmental Research

journal homepage: www.elsevier.com/locate/envres

Photocatalytic degradation and rate constant prediction of chlorophenols and bisphenols by $H_3PW_{12}O_{40}$/GR/TiO_2 composite membrane

Ying Ma[1], Yanan Zhang[1], Xiaolin Zhu, Nan Lu, Chao Li, Xing Yuan[*], Jiao Qu[**]

School of Environment, Northeast Normal University, Changchun, Jilin, 130024, China

ARTICLE INFO

Keywords:
Photocatalyst
Phenolic pollutants
Sol-gel
Degradation mechanism
Quantitative structure-activity relationship

ABSTRACT

Photocatalysis is a promising approach to remove highly toxic and refractory aromatics pollutants. However, developing highly active photocatalyst is a long-standing challenge for pollutant degradation. This study addressed this challenge by developing GR (graphene)/TiO_2 and HPW ($H_3PW_{12}O_{40}$)/GR/TiO_2 membranes by sol-gel method. The removal efficiencies of HPW/GR/TiO_2 (the doping of 1.0% HPW) membrane for chlorophenols (including o-chlorophenol, 2,4-dichlorophenol, 2,4,6-trichlorophenol, and pentachlorophenol) and bisphenols (such as Bisphenol A, Bisphenol AP, Bisphenol AF, and Bisphenol S) were up to 97.02–82.71% and 93.28–68.63% with simulated sunlight radiation for 5 h, respectively. Compared with GR/TiO_2 composite membrane, HPW/GR/TiO_2 remarkably accelerated the formation rates of $\cdot O_2^-$ and ·OH, due to the simultaneous transfer of photo-generated electrons (generated by TiO_2) to GR and HPW. In addition, the activity of the HPW/GR/TiO_2 membrane did not decline noticeably after 10-time recycle. Furthermore, the photocatalytic degradation reaction rate constants (k) of phenols by HPW/GR/TiO_2 membrane were calculated, and those for other chlorophenols and bisphenols were predicted using a quantitative structure-activity relationship model. The HPW/GR/TiO_2 membrane developed in this study poses high potential as an ideal photocatalyst for removal of phenolic pollutants in wastewater.

1. Introduction

Chlorophenols (CPs) are extensively used chemicals in daily life and their amounts present in wastewater are considerable (Prashanthakumar et al., 2018). CPs can severely affect human nervous and respiratory systems and cause serious hazards to human health. Odorous CPs in the environment have the persistence, toxicity, and carcinogenic characteristics (Fang et al., 2019; Yan et al., 2018a, 2018b). Bisphenols (BPs), a type of endocrine disrupting chemicals (EDCs), have attracted wide concern in the last few decades owing to its widespread application in industry (Romena et al., 2020). In recent years, BPs have caused various environmental problems including indoor dust, surface water, sediment, and wastewater (Shun et al., 2019). Moreover, the treated effluent from sewage treatment plants is a major source of BPs entering the aquatic environment (Salgueiro et al., 2019).

Titanium dioxide (TiO_2) has been used as a photocatalyst, due to its non-toxicity, high chemical activity, long-term stability, and relatively low cost (Fujishima et al., 2000; Yu et al., 2018). However, the rapid recombination of e-h^+ pairs is one key factor limiting the photocatalytic activity of TiO_2. An effective way to avoid the recombination of the e^--h^+ pair is to couple TiO_2 with other materials (Sánchez-Rodríguez et al., 2018; Khaki et al., 2017). Graphene (GR) could increase the separation efficiency of e^--h^+ pair as well as expand the optical absorption range of TiO_2 to the visible light region (Perera et al., 2012; Wang et al., 2013; Ma et al., 2016; Naderi et al., 2017; Martins et al., 2018; Ton et al., 2018; Xu et al., 2018), and enhance the photocatalytic activity of GR/TiO_2. Furthermore, POM (Polyoxometalate) has unique nanoscale and environmentally friendly transition metal-oxygen cluster, and exhibits superior photochemistry and reversible redox properties (Zheng et al., 2018). POM is a promising building block in the photocatalytic system and photovoltaic devices owing to the electronic transmission and storage. As a typical POM, $H_3PW_{12}O_{40}$ (HPW) could be an excellent candidate for delaying the e^--h^+ recombination on the surface of TiO_2 and improve the photocatalytic activity due to its intrinsic electronic attribution (Niu et al., 2018; Liu and Qu, 2017). Based on the structures and properties of TiO_2, GR, and $H_3PW_{12}O_{40}$, a HPW/GR/TiO_2 composite could be developed for advanced photocatalytic activity.

[*] Corresponding author.
[**] Corresponding author.
E-mail addresses: yuanx@nenu.edu.cn (X. Yuan), quj100@nenu.edu.cn (J. Qu).
[1] Ying Ma and Yanan Zhang contributed equally to this work.

https://doi.org/10.1016/j.envres.2020.109786
Received 14 January 2020; Received in revised form 30 April 2020; Accepted 3 June 2020
Available online 13 June 2020

Due to the continuous emergence of new pollutants, it is not realistic to investigate their degradation individually by using photocatalysis. Therefore, we predict the photocatalytic degradation of pollutants by models. Quantitative structure-activity relationship (QSAR) is efficient at correlating molecular structures of organic compounds with their "reactivity". However, QSAR has been limited to predict the toxicity and environmental process parameters of organic pollutants (Peric et al., 2015; Wang et al., 2015; Heo et al., 2019), while the prediction of the photocatalytic degradation reaction rate constant (k) values of pollutants has rarely been reported. Therefore, using the QSAR model established by the k values of pollutants to predict the k values of homologous pollutants is more practical.

In this work, GR was prepared using grass according to our previous study (Ma et al., 2016). GR/TiO_2 membranes were fabricated by sol-gel method that mixed the GR into TiO_2 solution. HPW/GR/TiO_2 membranes were prepared by doping HPW on GR/TiO_2 and loaded on the quartz plate. The photocatalytic degradations of GR/TiO_2 and HPW/GR/TiO_2 membranes for CPs (including O-chlorophenol, 2,4-dichlorophenol, 2,4,6- trichlorophenol, and pentachlorophenol) and BPs (such as Bisphenol A, Bisphenol AP, Bisphenol AF, and Bisphenol S) were also investigated. In addition, the mechanism of the photocatalytic degradation of phenolic pollutants using HPW/GR/TiO_2 was explored. Moreover, a QSAR model was improved to calculate the photocatalytic degradation reaction rate constants of HPW/GR/TiO_2 membranes for phenolic pollutants and predict the characteristic of photocatalytic degradation of it for other CPs and BPs.

2. Experiment

2.1. Preparation of the HPW/GR/TiO_2

The titanium tetraisopropoxide (TTIP) solution (denoted as A) was prepared by dropping 2 mL TTIP into 2 mL isopropanol with stirring for 1 h. 16 mg GR was added into 6 mL isopropanol and dispersed in ultrasonic for 1 h (denoted as B). The GR doping amount of the HPW/GR/TiO_2 membrane was 16 mg, since the photocatalytic activity of the GR/TiO_2 membrane (doping amount of GR was 16 mg) was the highest (shown in Fig. S1). Afterward, B was dropped into A under vigorous stirring. HPW powders (0.02 mmol, then the percentage of HPW in HPW/GR/TiO_2 was 1.0%) were added into isopropanol (1.6 mL) in ultrasonic for 1 h (denoted as C). C was added into the mixture solution of A and B and 0.5 mL acetic acid was added simultaneously for slowing down the hydrolysis rate of TTIP. The pH of the mixture was adjusted to 2–3 by hydrochloric acid (1 mol L^{-1}). After being stirred for 1 h at room temperature, the mixed solution was transferred into a 50 mL Teflon-lined reaction kettle, heated to 473 K with the heating rate of 2 K min^{-1}, kept at 473 K for 3 h, and cooled to room temperature at the cooling rate of 1 K min^{-1}, through which the HPW/GR/TiO_2 composite was obtained. In addition, the GR/TiO_2 membrane was also prepared as the control sample without addition of HPW. The doping ratio of GR to HPW in the HPW/GR/TiO_2 membrane was described in Fig. S1 of Supplementary Material.

The quartz substrate was treated in an ultrasound bath for 30 min (sequentially with detergent, ethanol, and distilled water) and dried at 333 K before use. The obtained composite was transferred into a 50 mL beaker and stirred (at 500 rpm for 6 s, and then at 2000 rpm for 20 s) for spin-coating on the quartz substrate (50 mm × 15 mm × 1 mm). Afterward, the HPW/GR/TiO_2 composite (about 5.0 mg) on the quartz substrate was aged at 293 K for 3 d.

2.2. Catalyst characterization

The prepared membranous composites were characterized using the following methods. Scanning electron microscope (SEM) images were taken using a Japan SII working at 20 kV. Energy dispersive spectra (EDS) were carried out with an Oxford EDS system attached to SEM. Transmission electron microscopy (TEM) and high-resolution TEM (HR-TEM) images were obtained using a Philips EM 208 working at 20 kV. X-ray diffraction (XRD) patterns were performed on a Rigaku D-max C III (Ni-filtered Al Kα radiation). X-ray photoelectron spectroscopy (XPS, Thermo ESCALAB 250) patterns were obtained using an Al Kα (λ = 0.83 nm, hμ = 1486.7 eV) X-ray source. Fourier transform infrared (FTIR) spectra (4000-400 cm^{-1}) were carried out using a Nexus 670 FTIR spectrometer (Thermo Nicolet, Madison) equipped with a KBr beam splitter (KBr, FT-IR grade). Raman spectra were obtained using a micro-Raman spectrometer (Nicolet Almega XR) with a 473 nm laser as an excitation source. Electron spin resonance (ESR) spectra were measured using a Bruker Elexsys E−580 electron spin resonance spectrometer, conducted at room temperature with the addition of 5,5-dimethyl-1-pyrroline N-oxide (DMPO, BePharm). In addition, EC550 electrochemical workstation (Wuhan Gaoss Union Technology Co., Ltd) was used to test the photocurrent of the composite membranes. The membranes tested, Pt wire, and Ag/AgCl (saturated $NaSO_4$ solution) were used as the working electrode, the counter electrode, and the reference electrode, respectively (Zhao et al., 2015). Additionally, the concentrations of phenolic pollutants were determined with High-Performance Liquid Chromatography (HPLC) equipped with a Dionex C-18 reversed-phase LC column (Waters Alliance HPLC). The HPLC conditions were shown in Table S1.

2.3. Photocatalytic degradation test

The light source (15 cm above the reactor) was provided by a Xe lamp (50 W, PLS-SXE300, Beijing Trusttech Co. Ltd., China). 100 mL CPs or BPs solution (5 mg L^{-1}) was poured into the quartz reactor, and the HPW/GR/TiO_2 composite membrane was immersed in the CPs or BPs solution which was kept in the dark with stirring for 30 min to achieve adsorption-desorption equilibrium. 1 mL solution, irradiated by the Xe lamp, was extracted and analyzed every 30 min for testing. The control experiment (photolysis) without the composites was also investigated. The k values were obtained by fitting the curves of ln (C_0/C_t) vs. irradiation time.

To investigate the photocatalytic degradation mechanisms of the HPW/GR/TiO_2 composites for CPs and BPs, 108 mg 4-benzoquinone (BQ, for $\cdot O_2^-$), 0.1 mL isopropanol (99.7%, for ·OH), and 3.7 mg ethylenediaminetetraacetic acid disodium salt (EDTA-2Na, for h^+) used as the radical scavenger, were added into the CPs and BPs solution, respectively. Furthermore, 0.4 mL methyl alcohol (99.5%) was used as the transforming agent for ·OH to $\cdot HO_2/\cdot O_2^-$ (Yao et al., 2008).

The recycling test of HPW/GR/TiO_2 membrane was used for the photocatalytic degradation of o-CP solution ten times under the same experimental conditions. The recycling HPW/GR/TiO_2 membrane was collected and used without any treatments in the next photocatalytic degradation processes during the entire experiment.

3. Results and discussion

3.1. Characterization of photocatalyst

The morphologies of GR/TiO_2 and HPW/GR/TiO_2 membranes were characterized using the SEM and TEM (Fig. 1). The layered GR in the membrane of GR/TiO_2 was observed (Fig. 1 a). However, the layered structure was indiscernible in the membrane of HPW/GR/TiO_2, indicating that GR was greatly reduced in the HPW/GR/TiO_2 composite (Fig. 1 b). Further analysis of the HRTEM images for GR/TiO_2 and HPW/GR/TiO_2 revealed that all the crystal lattice represented the TiO_2 (101) (Fig. 1c and d), and the crystal of TiO_2 was mainly anatase (insets of Fig. 1 c and d).

The characterization results showed the adsorption peaks of HPW at 799.39, 888.65, 984.92, and 1080.09 cm^{-1} in the FT-IR spectra (Fig. 2 a). The diffraction peaks (ranged from 1000 to 1600 cm^{-1}) were the O–Ti–O skeleton of TiO_2. The characteristic peaks at 1410 and

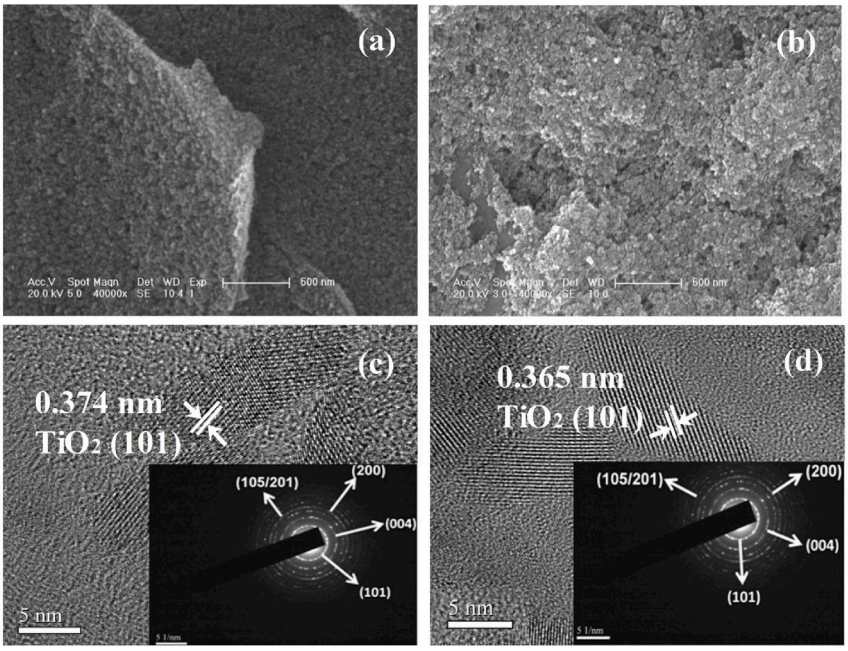

Fig. 1. SEM images of (a) GR/TiO_2 and (b) HPW/GR/TiO_2; HRTEM images of (c) GR/TiO_2 and (d) HPW/GR/TiO_2. The insets were SAED patterns.

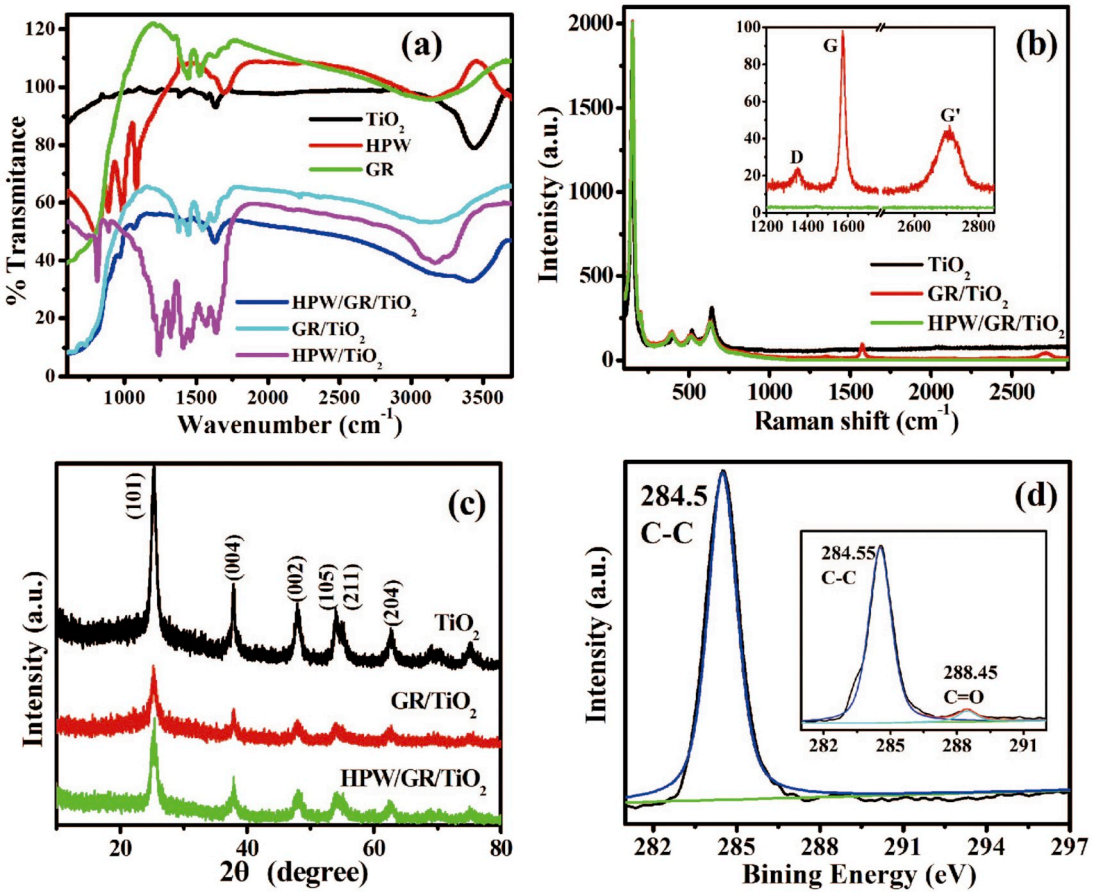

Fig. 2. (a) FT-IR spectrum of TiO_2, GR, HPW, HPW/TiO_2, GR/TiO_2 and HPW/GR/TiO_2; **(b)** Raman spectrum of TiO_2, GR/TiO_2 and HPW/GR/TiO_2 (Inset was Raman spectrum around the strongest peaks); **(c)** XRD patterns of the TiO_2, GR/TiO_2 and HPW/GR/TiO_2; **(d)** High-resolution XPS spectraum of HPW/GR/TiO_2 in the Cls: (Inset was GR/TiO_2 in the Cls).

1535 cm^{-1} represented C–OH and C═O of GR, respectively (Zhang et al., 2012). The two peaks at 946.72 and 1068.11 cm^{-1} in HPW/GR/TiO_2 displayed the $W=O_d$ and $P\text{-}O_a$. The peak at 1521 cm^{-1} (skeleton of C═O) was also observed in the composite. The diffraction peak at 1600 cm^{-1} was the skeleton of O–Ti–O. The peaks of HPW/GR/TiO_2 were broader than raw materials, indicating that the strong interaction

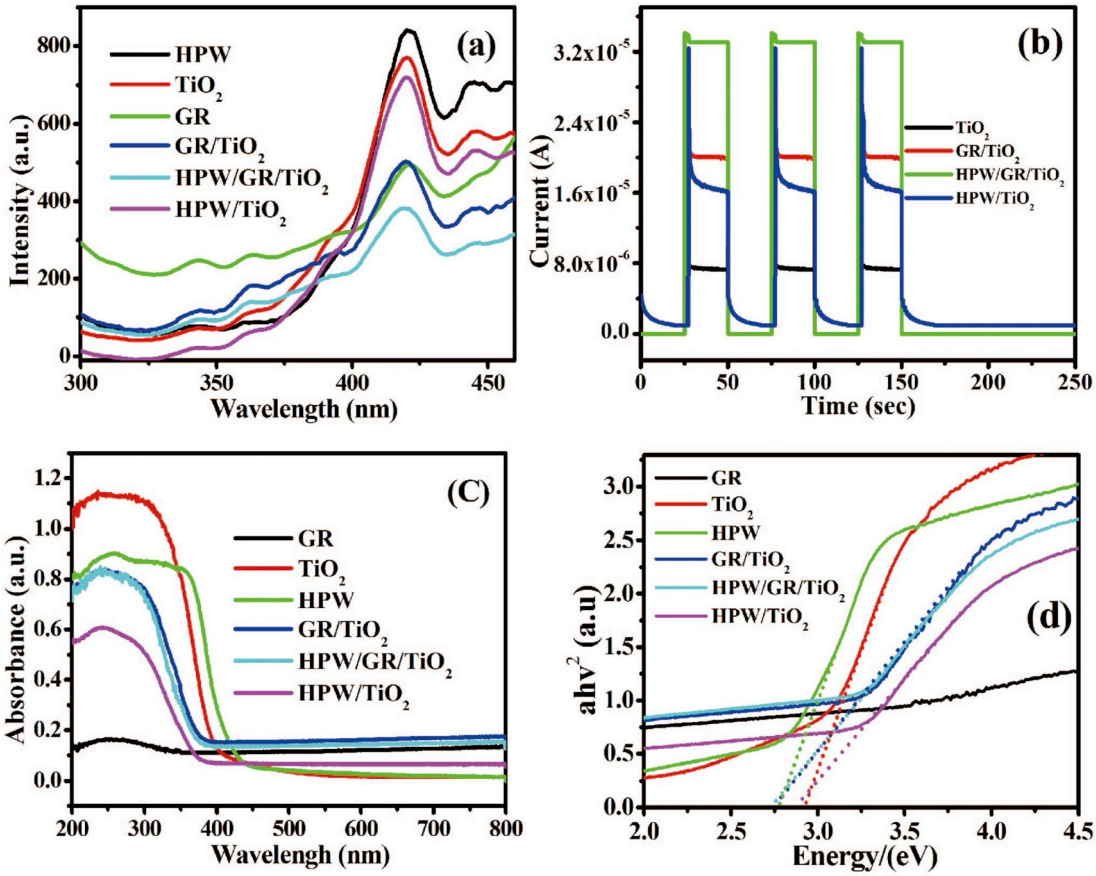

Fig. 3. (a) Room-temperature PL spectrum of TiO_2, GR, HPW, GR/TiO_2, HPW/TiO_2. and HPW/GR/TiO_2 under the excitation wavelength of 250 nm; (b) Photocurrent responses of TiO_2, GR/TiO_2, HPW/TiO_2 and HPW/GR/TiO_2; (c) UV–Vis/DRS spectrum and (d) Band gap of TiO_2, GR, HPW, GR/TiO_2, HPW/TiO_2 and HPW/GR/TiO_2.

among HPW, GR, and TiO_2. The peak at 1350.96 cm^{-1} (D band) was a common feature of sp^3 defects in carbon, which was associated with the structural defects of amorphous carbon (shown in Fig. 2 b). The peak at 1570.00 cm^{-1} (G band) corresponded to an E_{2g} mode of graphite related to the vibration of sp^2-bonded carbon atoms. The intensity ratio of these two bands was considered as a parameter for characterizing the quality of the carbon nanomaterials in the sample, and the high intensity ratio indicated the high degree of disorder in the carbon nanomaterials (Qu et al., 2015; Press-Kristensen et al., 2008). D/G intensity ratio (I_D/I_G) of GR/TiO_2 was 0.23, while the D and G peaks of HPW/GR/TiO_2 almost disappeared in the illustration. The peaks at 144, 394, 514, and 636 cm^{-1} of TiO_2 nanosheets were clear in Raman spectra. The percentage of exposed {001} facets in anatase TiO_2 was obtained by measuring the peak intensity ratio of the E_g (144 cm^{-1}) to A_{1g} (514 cm^{-1}) peaks (Hapeshi et al., 2010). The exposure ratios of TiO_2 {001} in TiO_2, GR/TiO_2, and HPW/GR/TiO_2 were 16.25, 11.40, and 15.23%, respectively. Although the {001} crystal surface exposure ratio of TiO_2 was the highest, its activity was still lower than that of HPW/GR/TiO_2 due to the absence of the co-catalyst. The peaks of TiO_2 were at $2\theta = 25.3^o$ (101), 37.9^o (004), 48.2^o (200), 53.9^o (105), 55.1^o (211), and 63.1^o (204) (Fig. 2 c), which were consistent with the characteristic peak of anatase. After coupling TiO_2 nanoparticles with HPW and GR, the intensities of these characteristic peaks decreased significantly, attributing to the homogeneous coverage of TiO_2 nanoparticles by GR and HPW. The oxygen-containing groups on the surface of GR disappeared in HPW/GR/TiO_2, meaning that GR was reduced completely (Fig. 2 d). The variation trend was consistent with the Raman spectra.

The characterization results of HPW/GR/TiO_2 and GR/TiO_2 materials XPS (Figs. S4 and S5) showed that the $Ti2p_{3/2}$ and $Ti2p_{1/2}$ binding energies of TiO_2 in the HPW/GR/TiO_2 were 458.8 and 464.6 eV, respectively, indicating that the Ti element in HPW/GR/TiO_2 was Ti^{4+}. Compared with the results in the GR/TiO_2 (Fig. S4 a), the Ti2p characteristic peak shifted to the high binding energy direction, which was caused by the decrease in the electron density around Ti after the addition of HPW. Compared to the GR/TiO_2 (Fig. S4 b), the characteristic peak of O1s in HPW/GR/TiO_2 (Fig. S5 b) did not changed substantially. Compared with HPW, the characteristic peaks in HPW/GR/TiO_2 (Fig. S5 c and d) dropped toward the low binding energy direction, indicating that the lost electrons from the Ti were attracted by the W. Therefore, the interaction in the interior of the composite was strong (Xu et al., 2010).

The photoluminescence spectra of materials, photo-excited with 250 nm light at room temperature, were generated from the recombination of electrons and holes (Fig. 3 a). The fluorescence emission of TiO_2, GR, and HPW were strong at 400–430 nm, and the center of emission peak was 420 nm. However, the peak strength of the HPW/GR/TiO_2 was the weakest, which suggested that separation efficiency of photo-generated electron and holes in HPW/GR/TiO_2 was the highest. All of TiO_2, GR, HPW, and HPW/GR/TiO_2 could generate a current signal rapidly with the illumination, and the signals were stable in photocurrent experiment (Fig. 3 b). The photocurrent signal of HPW/GR/TiO_2 was the largest owing to the highest separation efficiency of photo-generated electrons and holes.

UV–vis/DRS measurements were carried out to investigate the optical properties of the materials (Fig. 3 c and 3 d). Ranged from 200 to 400 nm, the absorption of TiO_2 and HPW for ultraviolet were strong broadband. With the addition of GR, the absorption wavelength of GR/TiO_2 and HPW/GR/TiO_2 were extended. In addition, the energy bands and absorption spectra of GR/TiO_2 and HPW/GR/TiO_2 were not changed significantly. From the characterization result of XPS (Fig. S4),

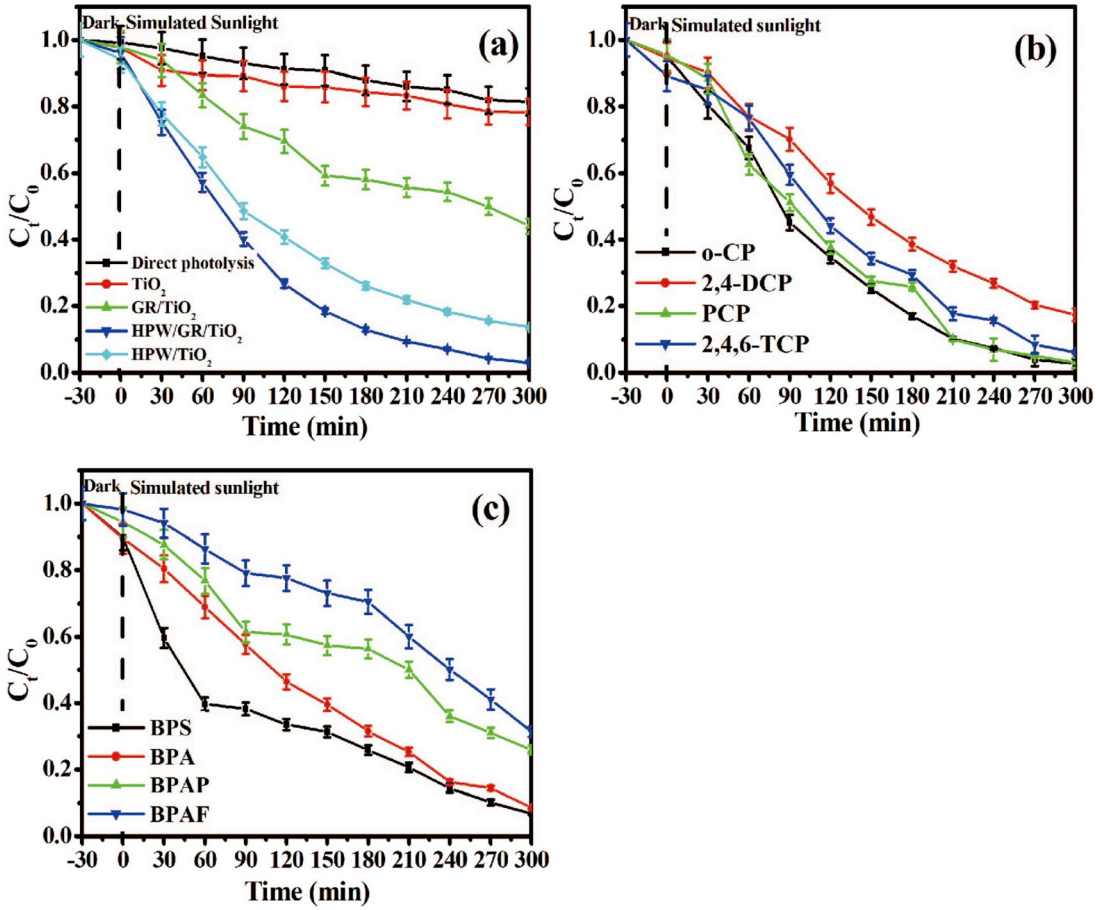

Fig. 4. (a) Photocatalytic degradations of TiO_2, GR/TiO_2, HPW/TiO_2 and $HPW/GR/TiO_2$ for o-CP; the photocatalytic degradations of $HPW/GR/TiO_2$ for (b) CPs and (c) BPs.

the GR in $HPW/GR/TiO_2$ was greatly reduced, resulting in the decreasing of the effective contact area between GR and TiO_2. However, the presence of HPW allowed the photo generated electron from TiO_2 to be transferred to HPW. Finally, the light absorption and energy band of the $HPW/GR/TiO_2$ were similar with GR/TiO_2.

3.2. Photocatalytic degradation of CPs and BPs by $HPW/GR/TiO_2$

Adsorption performance of $HPW/GR/TiO_2$ membrane to eight pollutants was studied to determine the role of adsorption in the photocatalysis process (Liu et al., 2019; Hu et al., 2020). The adsorption experiment of $HPW/GR/TiO_2$ membrane was carried out for 300 min. After 30 min, the adsorption processes of $HPW/GR/TiO_2$ membrane for CPs (Fig. S2 a) and BPs (Fig. S2 b) basically reached the adsorption-desorption equilibrium. The $HPW/GR/TiO_2$ membrane had an adsorption efficiency of 2.59–8.72% for CPs, and 0.32–9.42% for BPs. Therefore, 30 min was selected as the adsorption time.

The photocatalytic degradation efficiency of o-CP by $HPW/GR/TiO_2$ membrane with simulated sunlight irradiation for 300 min was significantly higher than TiO_2, GR/TiO_2 and HPW/TiO_2 (Fig. 4 a), which was consistent with the optical properties of the materials (Fig. 3). The order of removal rates of CPs was o-CP (97.02%) > 2,4,6-Trichlorophenol (2,4,6-TCP, 96.95%) > pentachlorophenol (PCP, 92.88%) > 2,4-Dichlorophenol (2,4-DCP, 82.71%) after being irradiated for 300 min (Fig. 4 b). For BPs, the order of the removal rate was Bisphenol S (BPS, 93.28%) > Bisphenol A (BPA, 91.39%) > Bisphenol AP (BPAP, 74.71%) > Bisphenol AF (PBAF, 68.63%) (Fig. 4 c).

In the photocatalytic degradation processes of $HPW/GR/TiO_2$ membrane for CPs and BPs, the hydroxylation was the initial degradation step (Zada et al., 2017; Yan et al., 2018a, 2018b; Ma et al., 2018). The degradation rate was related to the position and number of chlorine atom. The chlorine atom on the *para*-position was more difficult to be replaced compare with the *meta*- and *ortho*-position. Furthermore, the chlorine atom was easier to be replaced with the increasing number of chlorine atom on benzene ring. Therefore, the photocatalytic degradation for 2,4-DCP was the difficult.

For BPs, the diphenyl ring structure was relative stable, and the photocatalytic degradation efficiencies of $HPW/GR/TiO_2$ membrane for BPs was lower than for CPs (Fig. 4 a and b). The structure of BPAF was stable with the presence of C–F bond, the structure of the three benzene rings in BPAP led to the difficult initiation of the degradation.

The recyclability of the $HPW/GR/TiO_2$ membrane was evaluated by using o-CP as the target pollutant (Fig. S8). After ten times photocatalytic degradation experiments, the removal rates were 97.02%–94.33%, which suggested that the $HPW/GR/TiO_2$ membrane exhibited good stability and recyclability.

3.3. Photocatalytic activity mechanism of $HPW/GR/TiO_2$ to phenols

The ROS (reactive oxygen species) generated from the surface of TiO_2, GR/TiO_2 and $HPW/GR/TiO_2$ with simulated sunlight irradiation was determined using a DMPO spin-trapping ESR technique. These ESR signals with the intensity ratios of 1:2:2:1 and 1:1:1:1 represented the presence of DMPO-·OH and DMPO-$\cdot O_2^-$ adducts (Fig. 5 a and b) (Chen et al., 2015). Thus, ·OH and $\cdot O_2^-$ were involved in the photocatalytic degradation processes by TiO_2, GR/TiO_2, and $HPW/GR/TiO_2$. The formation efficiencies of ·OH and $\cdot O_2^-$ in GR/TiO_2 and $HPW/GR/TiO_2$

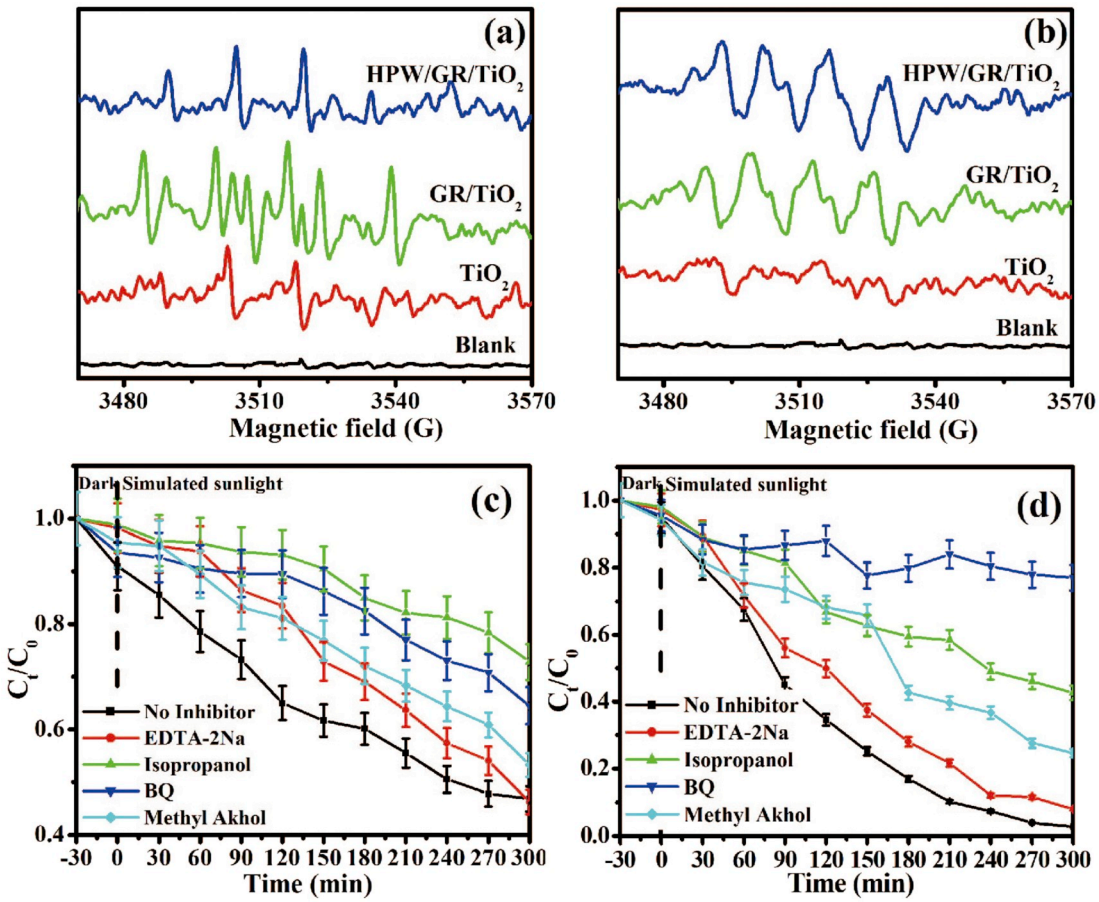

Fig. 5. ESR spectrum of the (a) DMPO-·OH and (b) DMPO-$\cdot O_2^-$ adducts recorded with TiO_2, GR/TiO_2 and $HPW/GR/TiO_2$; Plotted degradation curves of (c) GR/TiO_2 and (d) $HPW/GR/TiO_2$ for o-CP with the scavengers.

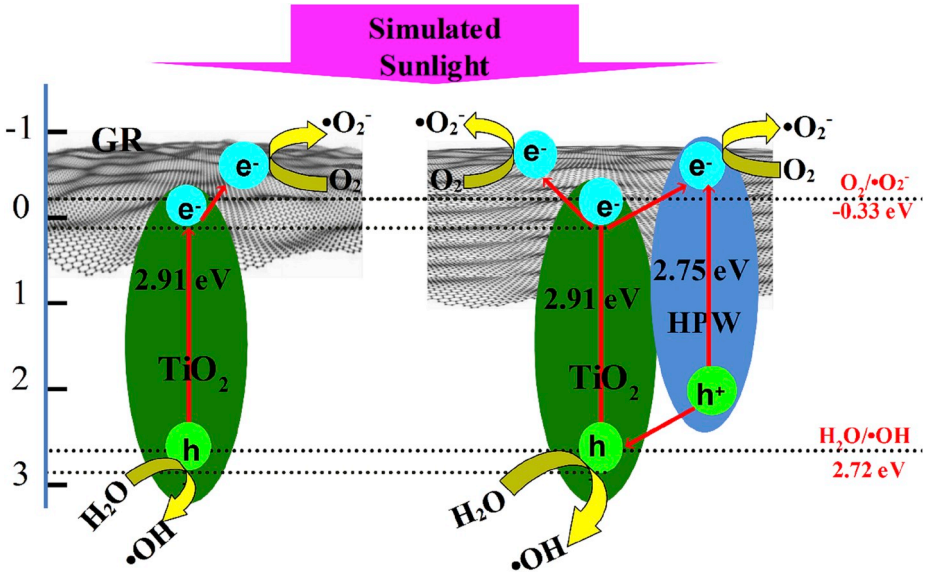

Fig. 6. Photocatalytic mechanisms of GR/TiO_2 and $HPW/GR/TiO_2$ membranes.

system were higher than TiO_2. The formation efficiencies of ·OH produced by $HPW/GR/TiO_2$ were lower than GR/TiO_2, while the formation efficiencies of $\cdot O_2^-$ was higher than GR/TiO_2.

The radical scavenger experiments of GR/TiO_2 and $HPW/GR/TiO_2$ were conducted (Fig. 5 c and d). The ·OH played an active role in the photocatalytic degradation of GR/TiO_2 for o-CP. The $\cdot O_2^-$ played the most important role and followed by ·OH in the photocatalytic degradation of $HPW/GR/TiO_2$ for o-CP. Therefore, the $\cdot O_2^-$ and ·OH were the most important ROS in the photocatalytic process, which was in accordance with the results of ESR characterization. The degradation path result of o-CP by $HPW/GR/TiO_2$ membrane was provided in the supplementary material (Figs. S6 and S7).

Table 1
The effect of radicals on the *k* values of phenolic compounds.

	Isopropanol(·OH)	BQ($\cdot O_2^-$)	Methyl alcohol (·OH transforming agent)	EDTA-2Na(h^+)	No Inhibitor
O-CP	0.0033	0.0007	0.0043	0.0081	0.0116
2,4-DCP	0.0024	0.0007	0.0025	0.0013	0.0061
2,4,6-TCP	0.0018	0.0049	0.0036	0.0039	0.0116
PCP	0.0065	0.0040	0.0097	0.0041	0.0098
BPA	0.0028	0.0012	0.002	0.0037	0.0070
BPAF	0.0010	0.0018	0.0024	0.0031	0.0033
BPAP	0.0010	0.0027	0.0027	0.0021	0.0040
BPS	0.0014	0.0007	0.0042	0.0068	0.0075

Table 2
Molecular structure descriptors and predicted *k* values of phenolic pollutants.

Compound	RDF060s	MATS5m	k_{pre} (min^{-1})
m-CP	1.281	−0.720	0.0223
p-CP	12.799	0.882	0.0036
2,5-DCP	0.005	0.669	0.0056
2,6-DCP	0	−0.402	0.0165
2,3,5-TCP	2.002	−0.477	0.0172
2,4,5-TCP	12.804	0.671	0.0045
BPB	46.399	0.015	0.0051
BPF	15.886	0.268	0.0065
TBBPA	18.970	0.037	0.0078
TBBPS	14.092	−0.165	0.0103

The mechanisms of photocatalytic degradation by GR/TiO_2 and HPW/GR/TiO_2 membranes (Fig. 6) showed that under the simulated sunlight, e^- was excited from the valence band (VB) of TiO_2 to the conduction band (CB), and h^+ generated on VB. In the GR/TiO_2, the photo generated electron from TiO_2 could be received by GR and combined with O_2 to form $\cdot O_2^-$ (Perera et al., 2012). In HPW/GR/TiO_2 system, the e^- would transfer to GR and HPW simultaneously and generate $\cdot O_2^-$, implying that the concentration of $\cdot O_2^-$ produced by HPW/GR/TiO_2 was higher than GR/TiO_2 (Fig. 5 b). At the same time, h^+ generated by HPW was also transferred to TiO_2 and generated ·OH.

To investigate the influence of ROS to the degradation for CPs and BPs, radical scavenger experiments were also carried out. The *k* values (Table 1) were inversely proportional to the contribution of ROS. The results showed that $\cdot O_2^-$, ·OH, and h^+ all contributed to the degradation of target pollutants. Photocatalytic degradation for o-CP, BPA, and BPS were mainly affected by $\cdot O_2^-$, nevertheless, 2,4,6-TCP and BPAP were mainly affected by ·OH. For 2,4-DCP degradation, $\cdot O_2^-$ and h^+ were the major active ROS. The $\cdot O_2^-$ and ·OH played the active roles in the degradation of BPAF. However, there was no significant difference in the contribution of ROS to the photocatalytic degradation for PCP. The reactive species generated in the photocatalytic system in this study played complex roles in the degradation of the target pollutants, which could be attributed to the structural differences (substituents or substituted positions) of these pollutants. The prepared membranes have different adsorption abilities toward these compounds with different structures, while the pollutants possess different reaction activities with these reactive species.

3.4. Photocatalytic property prediction of HPW/GR/TiO_2 to other CPs and BPs

The prepared HPW/GR/TiO_2 exhibited high catalytic activity toward the selected CPs and BPs, and the *k* values were shown in Table 1 (no inhibitor). The *k* values for the selected pollutants were structure-dependence. A QSAR model was developed with these *k* values based on the method described previously (Wang et al., 2015; Dong et al., 2010). The molecular structure descriptors of the selected pollutants were calculated by using Dragon software (Version 6.0) (Taletesrl, 2012). Equation (1) is the optimum multiple linear regression (MLR)-based QSAR models.

$$\log\ k = -1.960 - 0.007\ RDF060\ s - 0.441\ MATS5m \quad (1)$$

$$n = 8,\ R^2_{adj} = 0.970,\ Q^2_{Loo} = 0.875,\ RMSE = 0.039,\ K_x = 0.453,\ K_{xy} = 0.576.$$

where *n* represents the number of compounds in the training set; the descriptor RDF060s represents the radial distribution function-060/ weighted by I-state; MATS5m represents the Moran autocorrelation of lag 5 weighted by mass 2D autocorrelations. The R^2_{adj} for the QSAR models is 0.970, which suggests that the QSAR models reasonably fitted well with the training set. For internal validation, the Q^2_{Loo} is up to 0.875, indicating that the models are statistically robust (Tropsha et al., 2003). $K_x < K_{xy}$ and *VIF* < 2 (1.259 for RDF060s and MATS5m) for the selected descriptors suggest that both models are free of multi-collinearities. These results demonstrated that the model has high goodness-of-fit, robustness, and predictive ability.

The *k* values for other phenolic pollutants with similar molecular structures (Fig. S9) were predicted with the improved QSAR model. The results (Table 2) indicated these pollutants also possessed high *k* value, implying that the prepared HPW/GR/TiO_2 exhibited high catalytic activity toward other CPs and BPs. The *k* values were according to the follow order: *meta*-CP > *ortho*-CP > *para*-CP. Meanwhile, *k* values of DCP and TCP were consistent in the orders as follow: 2,6-DCP > 2,4-DCP, and 2,3,5-TCP > 2,4,6-TCP > 2,4,5-TCP. The prepared HPW/GR/TiO_2 also exhibited the highest catalytic activities toward other CPs with chlorine atom on the *meta*- and *ortho*-position compared with that on the *para*-position. The prepared HPW/GR/TiO_2 exhibited similar catalytic activity for BPs, except for BPAF that with the lowest *k* value (0.0033 min^{-1}). The stable C–F bond in BPAF resulted in slow degradation in the photocatalytic degradation processes. The prediction of the catalytic activities toward TBBPA (Tetrabromobisphenol A) and TBBPS (Tetrabromobisphenol S) showed that HPW/GR/TiO_2 exhibited high catalytic activity for these two pollutants, especially for TBBPS. The model calculation confirmed that the HPW/GR/TiO_2 composite was suitable for the treatment of wastewater containing CPs and BPs.

4. Conclusion

Novel HPW/GR/TiO_2 composite membrane was synthesized using the sol-gel method. Compared with GR/TiO_2, the addition of HPW accelerated the separation of the photo generated electron-hole pairs as well as enhanced the photocatalytic activity owing to the generation of a large number of ·OH and $\cdot O_2^-$ in the reactions. ·OH and $\cdot O_2^-$ were the main active reactive species for most CPs and BPs. However, there was no significant difference in the contribution of ROS to the photocatalytic degradation for PCP. The photocatalytic degradation rates of HPW/GR/TiO_2 for CPs and BPs were quite different, caused by their structural differences. In addition, the HPW/GR/TiO_2 displayed excellent catalytic stability and reusability due to strong interaction among HPW, GR, and TiO_2. More importantly, the successfully predicted *k* values of HPW/GR/TiO_2 for other CPs and BPs, using an improved QSAR model indicated that HPW/GR/TiO_2 was an excellent

photocatalyst for removal of CPs and BPs in wastewater.

CRediT authorship contribution statement

Ying Ma: Investigation, Writing - original draft. **Yanan Zhang:** Writing - original draft, Data curation. **Xiaolin Zhu:** Writing - review & editing. **Nan Lu:** Methodology. **Chao Li:** Data curation. **Xing Yuan:** Supervision, Writing - review & editing. **Jiao Qu:** Writing - review & editing.

Acknowledgement

The authors are grateful to the National Natural Science Foundation of China (51478097 and 51809044) and the Fundamental Research Funds for the Central Universities (2412018QD020).

Appendix A. Supplementary data

Supplementary data to this article can be found online at https://doi.org/10.1016/j.envres.2020.109786.

References

Chen, P., Lv, W., Chen, Z., 2015. Phototransformation of mefenamic acid induced by nitrite ions in water: mechanism, toxicity, and degradation pathways. Environ. Sci. Pollut. Res. 22, 12585–12596.

Dong, W., Lee, C.W., Lu, X., 2010. Synchronous role of coupled adsorption and photocatalytic oxidation on ordered mesoporous anatase TiO_2-SiO_2 nanocomposites generating excellent degradation activity of RhB dye. Appl. Catal. B Environ. 95, 197–207.

Fang, F., Run, Z.X., Su, N.W., 2019. Characterization of interactions between a metabolic uncoupler O-chlorophenol and extracellular polymeric substances of activated sludge. Environ. Pollut. 247, 1020–1027.

Fujishima, A., Rao, T.N., Tryk, D.A., 2000. Titanium dioxide photocatalysis. J. Photoch. Photobio. C. 1, 1–21.

Hapeshi, E., Achilleos, A., Vasquez, M.I., 2010. Drugs degrading photocatalytically: kinetics and mechanisms of ofloxacin and atenolol removal on titania suspensions. Water Res. 44, 1737–1746.

Heo, S.K., Safder, U., Yoo, C.K., 2019. Deep learning driven QSAR model for environmental toxicology: effects of endocrine disrupting chemicals on human health. Environ. Pollut. 253, 29–38.

Hu, J.S., Zhang, P.G., Cui, J.F., 2020. High-efficiency removal of phenol and coking wastewater via photocatalysis-Fenton synergy over a Fe-g-C_3N_4 graphene hydrogel 3D structure. J. Ind. Eng. Chem. 84, 305–314.

Khaki, M.R., Shafeeyan, M.S., Raman, A.A., 2017. Evaluating the efficiency of nano-sized Cu doped TiO_2/ZnO photocatalyst under visible light irradiation. J. Mol. Liq. 258, 354–365.

Liu, S., Qu, X., 2017. Construction of nanocomposite film of Dawson-type polyoxometalate and TiO_2, nanowires for electrochromic applications. Appl. Surf. Sci. 412, 189–195.

Liu, X.L., Xu, S., Chi, H.B., 2019. Ultrafine 1D graphene interlayer in g-C_3N_4/graphene/recycled carbonfiber heterostructure for enhanced photocatalytic hydrogen generation. Chem. Eng. J. 359, 1352–1359.

Ma, H.Y., Zhao, L., Wang, D.B., 2018. Dynamic tracking of highly toxic intermediates in photocatalytic degradation of pentachlorophenol by continuous flow chemiluminescence. Environ. Sci. Technol. 52, 2870–2877.

Martins, P.M., Ferreira, C.G., Silva, A.R., 2018. TiO_2/graphene and TiO_2/graphene oxide nanocomposites for photocatalytic applications: a computer modeling and experimental study. Compos. B Eng. 145, 39–46.

Ma, Y., Lu, N., Lu, Y., 2016. Comparative study of carbon materials synthesized "Greenly" for 2-CP removal. Sci. Rep-UK. 6, 29167–32981.

Naderi, H.R., Sobhaninasab, A., Rahiminasrabadi, M., 2017. Decoration of nitrogen-doped reduced graphene oxide with cobalt tungstate nanoparticles for use in high-performance supercapacitors. Appl. Sure. Sci. 423, 1025–1034.

Niu, P., Wang, D., Wang, A., 2018. Fabrication of bifunctional TiO_2/POM microspheres using a layer-by-layer method and photocatalytic activity for methyl orange degradation. J. Nanomater. 42, 12187–12195.

Perera, S.D., Mariano, R.G., Vu, K., 2012. Hydrothermal synthesis of graphene-TiO_2 nanotube composites with enhanced photocatalytic activity. ACS Catal. 2, 949–956.

Peric, B., Sierra, J., Esther, M., 2015. Quantitative structure–activity relationship (QSAR) prediction of (eco)toxicity of short aliphatic protic ionic liquids. Ecotoxicol. Environ. Saf. 115, 257–262.

Prashanthakumar, T.K.M., Kumar, S.K.A., Sahoo, S.K., 2018. A quick removal of toxic phenolic compounds using porous carbon prepared from renewable biomass coconut spathe and exploration of new source for porous carbon materials. J Environ Chem Eng 6, 1434–1442.

Press-Kristensen, K., Lindblom, E., Schmidt, J.E., 2008. Examining the biodegradation of endocrine disrupting bisphenol A and nonylphenol in WWTPs. Water Sci. Technol. 57, 1253–1256.

Qu, J., Zhang, Q., Xia, Y., 2015. Synthesis of carbon nanospheres using fallen willow leaves and adsorption of Rhodamine B and heavy metals by them. Environ. Sci. Pollut. Res. 22, 1408–1419.

Romena, S.S., Bruno, A.R., Jairo, L.R., Fernando Jr., B., Rapid, 2020. Sensitive and simultaneous determination of 16 endocrine-disrupting chemicals (parabens, benzophenones, bisphenols, and triclocarban) in human urine based on microextraction by packed sorbent combined with liquid chromatography tandem mass spectrometry (MEPS-LC-MS/MS). Chemosphere 240, 124951–124959.

Sánchez-Rodríguez, D., Medrano, M.G., Remita, H., 2018. Photocatalytic properties of BiOCl-TiO_2 composites for phenol photodegradation. Chem. Eng. 6, 1601–1612.

Salgueiro, J.N., Campillo, A., Viñas, L., Beiras, R., 2019. Occurrence of selected endocrine disrupting compounds in Iberian coastal areas and assessment of the environmental risk. Environ. Pollut. 249, 767–775.

Shun, L.J., Hui, M.L., Shuang, Z., 2019. Association of bisphenol A and its alternatives bisphenol S and F exposure with hypertension and blood pressure: a cross-sectional study in China. Environ. Pollut. 25, 113639–113650.

Taletesrl, 2012. Dragon (software for molecular descriptor calculation) version 6.0. http://www.talete.mi.it/.

Tropsha, A.P., Gramatica, V., Gombar, K., 2003. The importance of being earnest: validation is the absolute essential for successful application and interpretation of QSPR models. QSAR Comb. Sci. 22, 69–77.

Ton, N.N., Dao, A.T., Kato, K., 2018. One-pot synthesis of TiO_2/graphene nanocomposites for excellent visible light photocatalysis based on chemical exfoliation method. Carbon 133, 109–117.

Wang, Y., Chen, J., Yang, X., Lyakurwa, F., 2015. In silico model for predicting soil organic carbon normalized sorption coefficient (K_{OC}) of organic chemicals. Chemosphere 119, 438–444.

Wang, P., Wang, J., Wang, X., 2013. One-step synthesis of easy-recycling TiO_2-rGO nanocomposite photocatalysts with enhanced photocatalytic activity. Appl. Catal. B Environ. 132–133, 452–459.

Xu, L., Yang, E.M., Johansson, 2018. Photocatalytic activity and mechanism of bisphenol a removal over TiO_2-x/rGO nanocomposite driven by visible light. J. Chem. Eng. 350, 1043–1055.

Xu, L., Yang, X., Guo, Y.H., 2010. Simulated sunlight photodegradation of aqueous phthalate esters catalyzed by the polyoxotungstate/titania nanocomposite. J. Hazard Mater. 178, 1070–1077.

Yan, H., Huan, L., Qing, Z., Aimin, L., 2018a. New phenolic halogenated disinfection byproducts in simulated chlorinated drinking water: identification, decomposition, and control by ozone-activated carbon treatment. Water Res. 146, 298–306.

Yan, G., Xie, Q., Hongtao, Y., 2018b. Enhanced photocatalytic performance of a two-dimensional $BiOIO_3$/g-C_3N_4, heterostructured composite with a Z-scheme configuration. Appl. Catal. B Environ. 237, 947–956.

Yao, Y., Li, G., Ciston, S., Lueptow, R.M., Gray, K.A., 2008. Photoreactive TiO_2/carbon nanotube composites: synthesis and reactivity. Environ. Sci. Technol. 42, 4952–4957.

Yu, S.Q., Ling, Y.H., Wang, R.G., 2018. Constructing superhydrophobic WO_3@TiO_2 nanoflake surface beyond amorphous alloy against electrochemical corrosion on iron steel. Appl. Sure. Sci. 436, 527–535.

Zada, A., Qu, Y., Ali, S., 2017. Improved visible-light activities for degrading pollutants on TiO_2/g-C_3N_4, nanocomposites by decorating SPR Au nanoparticles and 2,4-dichlorophenol decomposition path. J. Hazard Mater. 342, 715–723.

Zhang, H., Xie, A., Shen, Y., 2012. Layer-by-layer inkjet printing of fabricating reduced graphene-polyoxometalate composite film for chemical sensor. Phys. Chem. Chem. Phys. 14, 12757–12763.

Zhao, Q., Chen, D., Li, Y., 2015. Rhodium complex immobilized on graphene oxide as an efficient and recyclable catalyst for hydrogenation of cyclohexene. Nanoscale 5, 882–885.

Zheng, H., Wang, C., Zhang, X., 2018. Control over energy level match in keggin polyoxometallate-TiO_2, microspheres for multielectron photocatalytic reactions. Appl. Catal. B Environ. 234, 79–89.